Fully Automatic Head Motion Correction for Interventional C-arm Systems using Fiducial Markers

Kerstin Müller, Martin Berger, Jang-Hwan Choi, Sanjit Datta,
Sonja Gehrisch, Teri Moore, Michael P. Marks, Andreas K. Maier, and Rebecca Fahrig

***Abstract*—Today, an angiographic C-arm CT system is standard in most interventional laboratories and 3-D imaging in the interventional suite has become common. Due to the longer acquisition time of a C-arm system, of up to several seconds, intra-scan patient motion is a problem. In this paper, a fully automatic motion estimation and compensation framework utilizing fiducial markers is presented to mitigate head motion during neuroradiology interventions. Involuntary head movement of the patient should be an easier problem to solve than motions such as cardiac and respiratory motion, but to date no practical solution has been integrated into a clinical C-arm CT system. Our framework consists of three major steps: marker detection with incorporated outlier removal, motion estimation and correction, and marker removal. The marker detection is based on an initial estimate of the marker position extracted from the motion-blurred filtered backprojection (FDK) reconstruction and on the fast radial symmetry transformed (FRST) 2-D projection images. The motion is estimated by the alignment of the forward projected 3-D initial marker positions to the actual detected 2-D marker positions. Here, a rigid motion model is used assuming no deformable transformation of the head. The head motion is then corrected in the filtered backprojection step. Finally, the detected markers can be removed in the 2-D projection images by simple interpolation. The framework was evaluated on three skull phantom datasets with and without induced motion during the scan, as well as on one clinical C-arm CT dataset. All 3-D reconstructions show a large improvement in image quality compared to the non-corrected 3-D reconstructions.**

I. Introduction

A. Purpose of this Work

Angiographic C-arm systems are the standard modality used during interventional procedures. Physicians can use 2-D fluoroscopic images from these systems for guidance and navigational support. In addition, newer systems permit cone-beam CT (CBCT), or the automated computation of 3-D volumes from rotational acquisitions [1]. CBCT acquisitions collect numerous high-resolution 2-D images over pre-defined angular range. However, the time necessary to acquire a sufficient number of 2-D images for 3-D reconstruction can be up to 20 seconds and is rarely below 5 seconds. At this time scale, involuntary motion such as cardiac, respiratory, and patient motion is unavoidable and can cause severe artifacts in the 3-D images. These artifacts can obscure important information and substantially decrease the clinical utility of the CBCT images. For example, in brain perfusion imaging using an interventional CBCT system [2], involuntary head motion degrades the quality of the resulting perfusion maps. Hence, in this paper a fully automatic, fiducial marker-based motion correction framework suitable for interventional neuroradiological applications is presented.

K. Müller, J.-H. Choi, and R. Fahrig are with the Department of Radiology, Stanford University, Stanford, CA, USA. email: kmuell@stanford.edu. M. Berger and A. K. Maier are with the Pattern Recognition Lab, Department of Computer Science, Friedrich-Alexander-Universität Erlangen-Nürnberg, Erlangen, Germany. A. K. Maier is also with the Erlangen Graduate School in Advanced Optical Technologies (SAOT), Erlangen, Germany. M. Berger is also with the Research Training Group 1773 "Heterogeneous Image Systems". S. Datta, S. Gehrisch, and T. Moore are with Siemens Medical Solutions USA, Inc. M. P. Marks is with the Department of Radiology and Neurosurgery, Stanford University, Stanford, CA, USA.

B. State-of-the-Art

In interventional imaging, motion estimation and compensation is an open, wide ranging, and complex problem. Most motion correction approaches are highly dependent on the motion pattern (rigid vs. deformable motion), the application (neuroradiology vs. cardiology), and specific geometric acquisition parameters (short vs. a full scan). Numerous iterative motion correction algorithms have been developed [3], that compare the forward-projected image to the original 2-D projection image according to a given similarity measure. In general, iterative methods provide a higher signal-to-noise ratio, but have higher computational costs.

Recently, several papers have been published employing data consistency conditions for motion estimation [4], [5], [6], [7]. Up to now, these techniques have not been applied to clinical data acquired with a C-arm system due to the limited scan range of about 200° and the cone-beam geometry. Hence, our framework uses fiducial markers to estimate the motion. Fiducial marker-based methods are advantageous because they do not rely on any trajectory assumptions and they do not require additional radiation or a prior CT scan. The idea of motion correction using fiducial marker detection has been already widely used in medical imaging [8], [9], [10], although to date the approach has not been implemented on a real clinical C-arm CT system. Therefore, we present a fully automatic motion estimation and compensation framework for CBCT head scans using fiducial markers.

II. Methods and Materials

A. 2-D Fiducial Marker Detection

As the first step, the fiducial markers attached to the patients head need to be detected in the individual 2-D projection images. Here, an automatic marker detection, presented by Berger et al. [11] is used. Berger et al. detected fiducial markers in a weight-bearing C-arm CT scan of a left knee.

First, the images are pre-processed with a morphological top-hat filter [12] in order to remove objects larger than the markers followed by a Sobel filter to enhance the remaining edges. Next, the fast radial symmetry transform (FRST) [13] is applied to the pre-processed 2-D images to detect the initial marker positions. The blurred FRST 2-D candidate points are backprojected to get a distinct outcome for each 3-D marker position. A binarisation step is performed using the maximum entropy method [14]. A 3-D connected component analysis is applied to identify the centroids of the marker positions in 3-D. With the help of the pre-calibrated projection matrices, $\boldsymbol{P}_j \in \mathbb{R}^{3\times4}$ for each projection image $j \in \{1,\dots,N\}$, with N the number of projection images, the 3-D reference markers can be forward projected onto each projection image yielding the 2-D reference points $\boldsymbol{r}'_{i,j}$, for each marker $i \in \{1,\dots,B\}$, with B denoting the number of markers. As a next step, a set of 2-D candidate points $\boldsymbol{m}_{i,j}$ are extracted from the initial FRST images, using a heuristically determined threshold and a 2-D connected-components analysis. These candidate points are then assigned to the closest 2-D reference points, essentially solving the correspondence problem. The 3-D marker positions can be updated by the newly assigned candidate points and the whole detection can be performed iteratively.

B. Outlier Removal

The detection of candidate points in the 2-D FRST processed projection images can lead to wrong marker positions, if for example, a marker in 2-D is overlayed by a high contrasted structure like a vessel. Therefore, 2-D outliers are removed before the motion estimation step. In order to detect the outlier, the 3-D motion trajectory of each marker (c.f. Figure 1a) is projected on the uz- and the vz-plane (c.f. Figure 1b), with u denoting the axis for the width and v the axis for the height of each projection image, and z the number of projections. For each 2-D marker trajectory a cubic smoothing spline is fitted to the original 2-D curve. If the distance of the original marker position to the new marker position is larger than a certain threshold, the point is considered an outlier. In Figure 1b, the 2-D original and smoothed motion trajectory of one marker on a skull phantom is illustrated. For motion estimation, the original motion trajectory is used.

C. 2-D/3-D Rigid Motion Estimation

For the estimation of the intra-scan motion based on the detected marker positions, the approach evaluated by Choi et al. [15], [16] in order to estimate knee motion during a weight-bearing C-arm scan is adapted. The algorithm estimates a 3-D rigid transformation for each projection image j, by fitting the forward projection of the 3-D reference marker position to the actual 2-D detected candidate points. The six degrees of freedom of each transformation matrix $\boldsymbol{M}_j \in \mathbb{R}^{4\times4}$, with

$$\boldsymbol{M}_j = \boldsymbol{T}_j(t_{x,j}, t_{y,j}, t_{z,j}) \cdot \boldsymbol{R}_z(\gamma_j) \cdot \boldsymbol{R}_x(\alpha_j) \cdot \boldsymbol{R}_y(\beta_j), \quad (1)$$

where $\boldsymbol{T}_j \in \mathbb{R}^{4\times4}$ is the translation and $\boldsymbol{R} \in \mathbb{R}^{4\times4}$ are the rotation matrices. In this paper, the unknown parameters are estimated by an interior-point optimizer [17], until the step size is smaller than 1e-3, with the given objective function:

$$\underset{t_{x,j},t_{y,j},t_{z,j},\gamma_j,\alpha_j,\beta_j}{\arg\min} \sum_{j=1}^{N}\sum_{i=1}^{B} ||\boldsymbol{r}'_{i,j} - \boldsymbol{m}_{i,j}||_2^2. \quad (2)$$

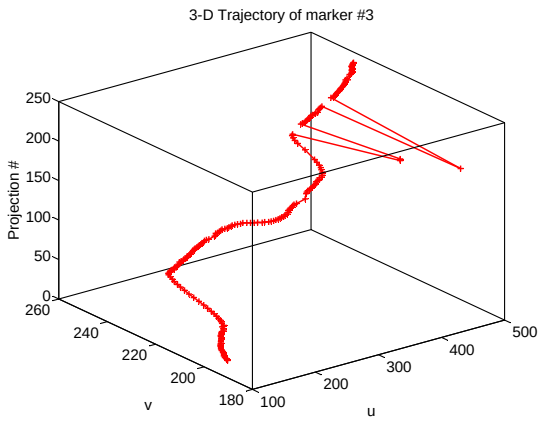

(a) Motion trajectory in 3-D.

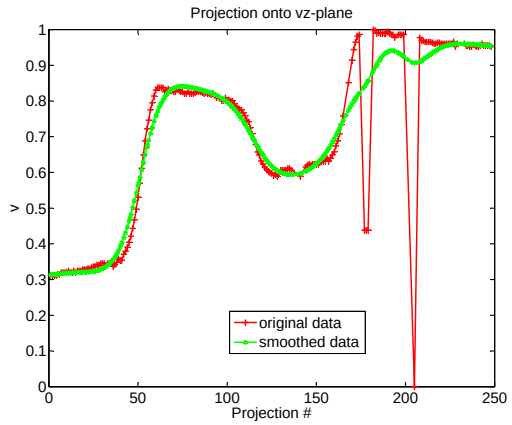

(b) Projection of 3-D motion trajectory onto the vz-plane. Original trajectory denoted with (+) in red and the fitted and smoothed cubic spline (*) in green.

Figure 1: 3-D and projected 2-D motion trajectory of marker #3 of a skull phantom with translational motion along the rotation axis.

In order to perform a motion-compensated reconstruction, each $\boldsymbol{M}_j$ rigid transformation matrix can be used to compute a new calibration matrix $\boldsymbol{P}_j^{new}$,

$$\boldsymbol{P}_j^{new} = \boldsymbol{P}_j \cdot \boldsymbol{M}_j, \quad (3)$$

with $\boldsymbol{P}_j$ denoting the pre-calibrated projection matrix for projection image j.

III. Experiments

A. Head Phantom

The presented framework was evaluated using a skull phantom with contrasted vessels in the right hemisphere (see Figure 2a). The skull phantom was scanned using an Artis zeego system (Siemens AG, Healthcare Sector, Forchheim, Germany). An interventional CBCT head scan acquisition protocol was used, with the following scanning parameters: the scan time was 5 s acquiring 248 images at 60 f/s, and with an angular increment of 0.8° during one C-arm sweep. The isotropic

Table I: The minimal, maximal, mean and standard deviation, and median number of markers detected on the three head phantom scans.

Dataset	Min	Max	Mean ± Std	Median
No motion	4	7	6.60 ± 0.64	7
Translation	5	7	6.39 ± 0.65	6
Rotation	5	7	6.60 ± 0.60	7
	4.67 ± 0.58	7	6.53 ± 0.63	

pixel resolution was 0.616 mm/pixel (0.40 mm at isocenter) and the detector size 480 × 620 pixels. A dose of 0.36 μGy/f at the detector was applied. Image reconstruction was performed with a sharp reconstruction kernel on an image volume of $(25.6\text{ cm})^3$ distributed on a 256^3 voxel grid. Three different scans with different induced motion patterns were performed, (1) without any motion, (2) with translational motion ($\pm$1 cm) along, and (3) with rotational motion ($\pm 10^\circ$) around the rotation axis of the C-arm. Seven 7 X-SPOT® radiopaque pellets from Beekley Medical™ with 1.5 mm diameter, widely used in neuroradiology, were attached to the head phantom ensuring that the markers would not overlap on any individual projection images during the C-arm rotation.

B. Clinical Data

One patient dataset was acquired on an Artis zee biplane system (Siemens AG, Healthcare Sector, Forchheim, Germany), using only one detector plane. The same scanning parameters as for the skull phantom, described in Section III-A were applied. Only three tantalum beads with a diameter of 1 mm were attached to the patient's head, again to avoid overlapping in different 2-D projection images.

IV. Results and Discussion

A. Marker Detection and Outlier Removal

1) Head Phantom: For the skull phantom with the induced motion patterns, the stability of the marker detection was evaluated. Table I shows the minimal and maximal number of markers, as well as the mean and median number, detected over all $N = 248$ projection images. Even in the static dataset, some projections had as few as 4 markers detected due to overlap of the others with contrast-filled vessels and rounded vessel bifurcations that can mislead the detection process. On average for all three phantom scans, 6.53 ± 0.63 markers from a total of 7 markers were detected over the whole scan.

Table II shows the effect of the outlier removal on the accuracy of the marker detection process. The error ϵ denotes the deviation between the forward projected 3-D reference points and the 2-D detected candidate points in the FRST images. The deviation ϵ_{trans} denotes the error after the transformation of the 3-D reference points according to the motion estimation process and the 2-D detected candidate points in the FRST images. On average, applying motion correction with outlier removal results in a ≈93 % reduction in the marker distances relative to the uncorrected data, if motion was present in the scan. All outliers are successfully detected, except four outliers at the beginning of the scan with the induced translational motion.

Table II: The mean error ϵ defines the error between the forward projected 3-D reference points and the detected 2-D candidate points on the FRST images and the mean error ϵ_{trans} between the transformed forward projected 3-D reference points.

No Outlier Detection			
Dataset	ϵ	ϵ_{trans}	% improvement
No motion	0.50± 0.31	0.41± 0.39	18 %
Translation	12.16± 5.79	1.43 ± 1.52	88 %
Rotation	11.96± 8.55	0.49 ± 0.42	96 %
Outlier Detection			
Dataset	ϵ	ϵ_{trans}	% improvement
No motion	0.48 ± 0.19	0.37 ± 0.12	23 %
Translation	12.09 ± 5.73	1.20 ± 0.73	90 %
Rotation	11.94 ± 8.56	0.45 ± 0.11	96 %

2) Clinical Data: In the clinical dataset, a minimum of one marker and a maximum of all three markers were detected in the 2-D projection images. On average, 2.81 ± 0.41 markers were detected over the whole acquisition. No outliers were detected in the dataset.

B. Visual Inspection

1) Head Phantom: Figure 2b shows a representative slice of the 3-D reconstruction of the skull phantom without any induced motion for reference. The 3-D reconstruction of the phantom with translational motion, but no motion correction is illustrated in Figure 2c and the corresponding reconstruction with motion correction is shown in Figure 2d. The skull bone can be successfully reconstructed after the motion correction step. The same can be seen for the phantom with the induced rotational motion (Figure 2e and 2f).

2) Clinical Data: The clinical dataset shows only small motion artifacts in the standard FDK reconstruction (Figure 3a), primarily around the sphenoid bone and the occipital bone (marked by the arrows). These artifacts are reduced by the motion correction, as shown in Figure 3b.

V. Conclusion

In this paper, we presented a fully automatic motion estimation and compensation framework for neuroradiological data using a C-arm CT system utilizing fiducial markers. The resulting image quality is considerably improved compared to standard FDK reconstructions with no motion correction. The results on the skull phantom as well as on the clinical patient dataset are promising and encourage to implement our framework in a clinical environment.

Disclaimer: The concepts and information presented in this paper are based on research and are not commercially available.

Acknowledgment

The authors gratefully acknowledge funding support from the NIH Shared Instrument Grant S10 RR026714 supporting the zeego@StanfordLab, and Siemens AX. The authors also gratefully acknowledge funding of the Research Training Group 1773 "Heterogeneous Image Systems" and the Erlangen Graduate School in Advanced Optical Technologies (SAOT) by the German Research Foundation (DFG).

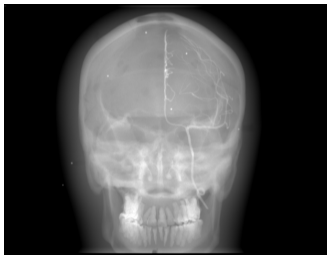

(a) Posterior 2-D projection of the skull phantom with attached markers.

(b) without motion

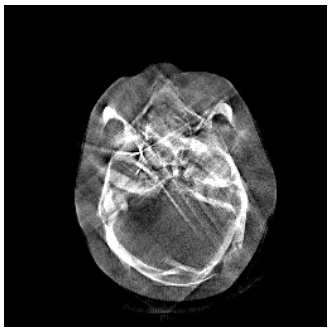

(c) with translational motion without motion correction

(d) with translational motion with motion correction and marker removal

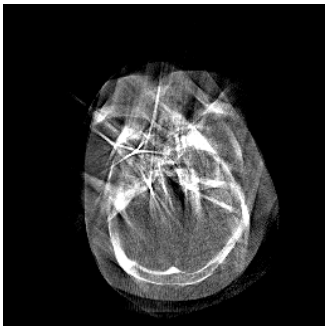

(e) with rotational motion without motion correction

(f) with rotational motion with motion correction and marker removal

Figure 2: Skull phantom (a) and axial slices 13 mm from the central slice of the 3-D reconstructions without (b) and with different motion patterns (c,d) and the corresponding motion corrected reconstructions (e,f) (W 1800 HU C 366 HU).

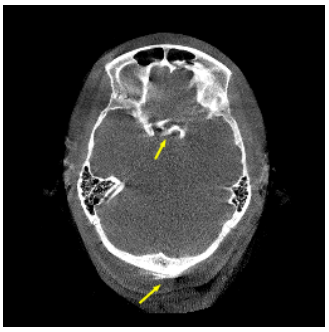

(a) no motion correction

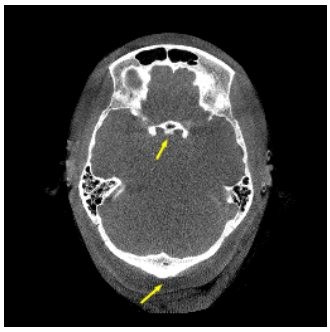

(b) motion correction

Figure 3: Axial slices 22 mm from the central slice of the 3-D reconstruction without (a) and with motion correction (b) of the clinical dataset (W 1900 HU C 406 HU).

REFERENCES

[1] L. Feldkamp, L. Davis, and J. Kress, "Practical cone-beam algorithm," *J Opt Soc Am A*, vol. 1, no. 6, pp. 612–619, 1984.

[2] M. T. Manhart, M. Kowarschik, A. Fieselmann, Y. Deuerling-Zheng, K. Royalty, A. K. Maier, and J. Hornegger, "Dynamic Iterative Reconstruction for Interventional 4-D C-Arm CT Perfusion Imaging," *IEEE Trans Med Imag*, vol. 32, no. 7, pp. 1336–1348, 2013.

[3] C. Bodensteiner, C. Darolti, H. Schumacher, L. Matthäus, and A. Schweikard, "Motion and Positional Error Correction for Cone Beam 3D-Reconstruction with Mobile C-Arms," in *Medical Image Computing and Computer-Assisted Intervention - MICCAI 2007*, 2007, pp. 177–185.

[4] N. Maass, F. Dennerlein, A. Aichert, and A. Maier, "Geometrical Jitter Correction in Computed Tomography," in *Proceedings of the Third International Conference on Image Formation in X-Ray Computed Tomography*, 2014, pp. 354–358.

[5] M. Berger, A. Maier, Y. Xia, J. Hornegger, and R. Fahrig, "Motion Compensated Fan-Beam CT by Enforcing Fourier Properties of the Sinogram," in *Proceedings of the Third International Conference on Image Formation in X-Ray Computed Tomography*, 2014, pp. 329–332.

[6] A. Aichert, N. Maass, Y. Deuerling-Zheng, M. Berger, M. Manhart, J. Hornegger, A. K. Maier, and A. Doerfler, "Redundancies in X-ray Images Due to the Epipolar Geometry for Transmission Imaging," in *Proceedings of the Third International Conference on Image Formation in X-Ray Computed Tomography*, 2014, pp. 333–337.

[7] W. Wein and A. Ladikos, "Towards General Motion Recovery in Cone-Beam Computed Tomography," in *Proceedings of the Fully Three-Dimensional Image Reconstruction in Radiology and Nuclear Medicine*, 2013, pp. 54–57.

[8] M. W. Jacobsen and J. Stayman, "Compensating for Head Motion in Slowly-Rotating Cone Beam CT Systems with Optimization Transfer Based Motion Estimation," in *Proceedings of the Nuclear Science Symposium Conference*, 2008.

[9] S. Sawall, M. Knaup, and M. Kachelriess, "A Robust Geometry Estimation Method for Spiral, Sequential and Circular Cone-Beam Micro-CT," *Med Phys*, vol. 39, no. 9, pp. 5384–5392, 2012.

[10] J. H. Kim, J. Nuyts, Z. Kuncic, and R. Fulton, "The Feasibility of Head Motion Tracking in Helical CT: a Step Toward Motion Correction," *Med Phys*, vol. 40, no. 4, p. 041903, 2013.

[11] M. Berger, C. Forman, C. Schwemmer, J.-H. Choi, K. Mueller, A. Maier, J. Hornegger, and R. Fahrig, "Automatic Removal of Externally Attached Fiducial Markers in Cone Beam C-arm CT," in *Bildverarbeitung für die Medizin 2014*, 2014, pp. 168–173.

[12] E. Hansis, H. Schomberg, K. Erhard, O. Doessel, and M. Grass, "Evaluation of Iterative Sparse Object Reconstruction From Few Projections for 3-D Rotational Coronary Angiography," *IEEE Trans Med Imag*, vol. 27, no. 11, pp. 1548–1555, 2008.

[13] G. Loy and A. Zelinsky, "Fast Radial Symmetry for Detecting Points of Interest," *IEEE Trans Pattern Anal Mach Intell*, vol. 25, no. 8, pp. 959–973, 2003.

[14] J. Kapur, P. K. Sahoo, and A. Wong, "A New Method for Gray-Level Picture Thresholding Using the Entropy of the Histogram," *Computer vision, graphics, and image processing*, vol. 29, no. 3, pp. 273–285, 1985.

[15] J.-H. Choi, R. Fahrig, A. Keil, T. F. Besier, S. Pal, E. J. McWalter, G. S. Beaupre, and A. Maier, "Fiducial Marker-Based Correction for Involuntary Motion in Weight-Bearing C-arm CT Scanning of Knees. Part I. Numerical Model-Based Optimization," *Med Phys*, vol. 40, no. 9, p. 091905, 2013.

[16] J.-H. Choi, A. Maier, A. Keil, S. Pal, J. McWalter, G. S. Beaupre, G. E. Gold, and R. Fahrig, "Fiducial Marker-Based Correction for Involuntary Motion in Weight-Bearing C-arm CT Scanning of Knees. II. Experiment," *Med Phys*, vol. 41, no. 6, p. 061902, 2014.

[17] R. H. Byrd, M. E. Hribar, and J. Nocedal, "An Interior Point Algorithm for Large-Scale Nonlinear Programming," *SIAM J Optimiz*, vol. 9, no. 4, pp. 877–900, 1999.